

Ionospheric and Solar Wind Contributions to the Storm-time Near-Earth Plasma Sheet

Lynn M. Kistler¹

¹University of New Hampshire

November 24, 2022

Abstract

The storm-time ring current is formed by the inward convection of the near-earth plasma sheet, so understanding the changing source of the plasma sheet is key for understanding ring current development. The ionospheric and solar wind sources can be distinguished by the charge state of the heavy ions; solar wind ions are highly ionized, while ionospheric ions are predominantly singly ionized. AMPTE/CHEM measurements are used to track the changing composition in the 6-9 Re plasma sheet as a storm develops in order to determine the fraction of the population that comes from each source. We find that prior to the storm, the solar wind source dominates. The source transitions sharply to ionospheric plasma during the storm main phase, and returns to solar wind plasma during the recovery phase.

Ionospheric and Solar Wind Contributions to the Storm-time Near-Earth Plasma Sheet

L. M. Kistler¹

¹University of New Hampshire.

Corresponding author: Lynn M. Kistler (Lynn.Kistler@unh.edu)

Key Points:

- Contributions of ionospheric and solar wind plasma to the near-earth plasma sheet are tracked during one storm using the AMPTE/CHEM instrument.
- There is a sharp change from a predominantly solar wind to ionospheric source during each storm main phase.
- The source changes back to solar wind during the recovery phase.

Abstract

The storm-time ring current is formed by the inward convection of the near-earth plasma sheet, so understanding the changing source of the plasma sheet is key for understanding ring current development. The ionospheric and solar wind sources can be distinguished by the charge state of the heavy ions; solar wind ions are highly ionized, while ionospheric ions are predominantly singly ionized. AMPTE/CHEM measurements are used to track the changing composition in the 6-9 Re plasma sheet as a storm develops in order to determine the fraction of the population that comes from each source. We find that prior to the storm, the solar wind source dominates. The source transitions sharply to ionospheric plasma during the storm main phase, and returns to solar wind plasma during the recovery phase.

Plain Language Summary

The ions trapped in the earth's magnetic field have two possible sources: the sun, or the earth's ionosphere. A stream of ionized particles from the sun called the solar wind is constantly moving outward, flowing by the earth. These particles can enter the earth's magnetosphere, and become trapped. Ions can also be accelerated out of the ionosphere into the magnetosphere. The interplay between these two sources is not well understood. In this paper, we test how the source changes as a large geomagnetic storm develops. We find that the source switches from being almost completely solar wind, to almost completely ionospheric during the peak of the storm.

1 Introduction

The enhancement of the ring current during a geomagnetic storm is predominantly due to the inward convection of the near-earth plasma sheet. Therefore, the source of the near-earth plasma is critical in determining the composition of the ring current. Both the solar wind and the ionosphere can be sources for the plasma sheet. Wing et al. (2014) has summarized our current knowledge of solar wind entry and transport to the plasma sheet. The plasma sheet spectrum during northward IMF is often well-described by a two-component Maxwellian. Generally, the colder component in the plasma sheet is identified as a solar wind component because it is similar in temperature to the adjacent magnetosheath plasma and has its highest occurrence towards the flanks. In general, this cold dense plasma sheet occurs after several hours of northward IMF, and is observed predominantly near the flanks and at high magnetic latitudes (Oieroset et al., 2003). The source of the hotter component could either be from the ionosphere or from the solar wind plasma that has entered farther down the tail and been heated during its transport. The cold population has likely entered more directly from the magnetosheath, either at the dayside through double cusp or lobe reconnection, or through the flanks, aided by Kelvin-Helmholtz instabilities or kinetic Alfvén waves. Simulations of ion entry during northward IMF (Sorathia et al., 2019) indicate that the cold population enters predominantly through the flanks through Kelvin-Helmholtz instability, while the cusp entry leads to a hotter population. During southward IMF, there can also be a maximum in the cold density along both flanks, but the density is smaller than during northward IMF. Thomsen et al. (2003) and Lavraud and Jordanova (2007) explored the transition when a period of northward IMF is followed by a strongly southward IMF, driving a storm. They have suggested that this dense plasma can load the near-earth plasma sheet, and then get driven into the inner magnetosphere when the IMF turns

southward, creating a strong ring current. This would imply that at least at the beginning of a storm, the ring current is formed by solar wind plasma.

The ionospheric plasma also has access to the plasma sheet. Ion outflow over a range of energies occurs throughout the auroral oval and in the polar cap. In the polar cap, the ion escape is mainly due to the ambipolar electric field. In the auroral regions, local wave acceleration energizes ionospheric plasma to higher energies. O^+ from both the nightside auroral region and dayside cusp regions are observed entering the plasma sheet during storms (Kistler et al. 2019, Kistler et al., 2016, Kistler et al., 2010). The occurrence frequency of O^+ in the lobe transported from the cusp increases with geomagnetic activity (Liao et al., 2010). Cold (~ 10 eV) ionospheric H^+ is also observed in the lobe (Engwall et al., 2006). Trajectory tracing shows that its most likely source is outflow from the polar cap (Li et al., 2012), and that about 85% of these ions are deposited in the plasma sheet (Li et al., 2013). Statistical studies have shown that the O^+ content of the plasma sheet increases with both geomagnetic activity (Kp) and solar EUV (F10.7), (Young et al., 1982, Mouikis et al., 2010). Studies of the storm-time ring current (e.g. Hamilton et al., 1988, Greenspan and Hamilton, 2002, Mouikis et al. 2019) have shown that a significant fraction of the energy density of the storm-time ring current is carried by O^+ , indicating the importance of the ionospheric source.

Thus, observations indicate that both sources play a role in the plasma sheet, and both have been suggested as sources of the storm-time ring current. But how the source contributions change in time and which source dominates at any time, particularly as a storm develops, is not well understood. Composition is one tool that can be used to distinguish the sources. The dominant species in the plasma sheet is hydrogen, and hydrogen can come from either the solar wind or from the ionosphere. However, the heavy ion contributions to the two sources are significantly different. The solar wind heavy ions are highly ionized, with He^{++} the second most abundant species at $\sim 4\%$ and a contribution from high charge state Carbon, Nitrogen and Oxygen, of $< 0.1\%$ percent, with O^{+6} the most abundant of the group. The ionospheric heavy ions are predominantly singly ionized, with O^+ the most abundant, followed by N^+ and He^+ . Thus, an analysis of the plasma sheet minor ion composition that includes charge state analysis can help to determine the plasma sheet source.

To quantitatively use the minor ions to determine the full source contribution requires knowing what fraction of the population is carried by the minor ions. For the ionospheric component, that fraction is highly variable. The O^+ component of the auroral outflow exhibits much stronger variability than the H^+ [e.g. Yau and Andre, 1997]. In addition, the ionospheric outflow can come from the polar cap, the cusp or the night-side aurora and the composition ratios of the outflow in those regions are all different (e.g. Yau et al, 2007, Wilson et al, 2004, Zhao et al., 2020). In addition, the transport to the tail from the cusp depends on the velocity, with higher velocity ions making it further down the tail than lower velocity ions. Thus, for ions leaving the cusp at the same energy, the O^+ will enter the plasma sheet closer to the earth than the H^+ , and so the composition ratio in the plasma sheet at a particular location depends critically on the energy spectrum in the outflow region, as well as the outflow flux. Therefore, while O^+ is a definitive tracer of an ionospheric contribution to the plasma sheet, there is no fixed O^+/H^+ ratio for the ionospheric source that can be used to determine how much of the H^+ is from the ionosphere, based on the amount of O^+ present.

While the fraction of minor ions in the solar wind is also not constant, its range of variability is smaller than the range of variability of the ionospheric source. Kasper et al., (2007)

and (2012) have examined the $\text{He}^{++}/\text{H}^+$ ratio as a function of both solar cycle and solar wind speed. They find that the ratio in the slow solar wind varies with solar cycle from about 1% at solar minimum to 4% at solar maximum, while the ratio in the fast solar wind is more constant, at around 4%. At solar minimum the $\text{He}^{++}/\text{H}^+$ ratio increases approximately linearly with speed. The heavier ion solar wind abundances for slow and fast wind were examined by von Steiger et al. (2000) using Ulysses/SWICS data and Lepri et al., (2013), using ACE/SWICS data. The Ulysses dataset included slow wind near the heliographic equator for both solar minimum and solar maximum, and fast wind towards the poles for solar minimum. The ACE dataset included a full solar cycle, measured close to the ecliptic plane at L1. Von Steiger et al. (2000) presented the abundances, including the Helium abundance, relative to Oxygen, not to H^+ . In this representation, they found no systematic difference in the slow wind relative abundances between solar maximum and solar minimum. This implies that the differences reported by Kasper for He^{++} (ie. the increase from minimum to maximum) are present for all the minor ions. Lepri et al., (2013) confirmed that the increase in all the heavy ion abundances relative to protons from min to max for the slow solar wind is about the same. For a given phase of the solar cycle and type of wind, the Lepri et al. (2013) results give abundances relative to protons and a variation about the mean that can be used to estimate the expected number of protons, based on the heavy ions.

There are a few caveats in using average solar wind values to estimate the fraction of the H^+ that comes from the solar wind. The first is that it assumes that the solar wind composition is unchanged when it enters the magnetosphere. This has not been proven definitively, but there are indications that it is true. Gloeckler and Hamilton (1987) found that the $\text{He}^{++}/\text{CNO}^{>3+}$ ratio in the plasma sheet was consistent with an average solar wind value. Recently, Delano et al., (2019), used MMS data to test whether the $\text{He}^{++}/\text{H}^+$ ratio was preserved across the magnetopause when reconnection occurs and found that it was. Thus, while there is certainly more room for study on this, this assumption seems reasonable. A second caveat is that the solar wind structures that drive a storm are not simply slow or fast wind. They are likely either a stream interface or a coronal mass ejection (CME). Solar wind plasma in CMEs sometimes has He^{++} enhancements, and other heavy ions can be enhanced as well (Galvin, 1997, Zurbuchen et al., 2006). Thus ideally, it would be best to have simultaneous solar wind measurements to make the comparisons. However, even without simultaneous solar wind measurements, reasonable estimations can be made.

While instrumentation on recent magnetospheric missions (e.g. MMS, Van Allen Probes) have improved over previous instruments in terms of time resolution and background rejection, they have not emphasized high mass or mass per charge resolution, and generally measure either mass per charge, without distinguishing mass, or measure mass, without distinguishing charge state. To measure solar wind minor ions other than He^{++} , it is necessary to distinguish both. The Charge Energy Mass (CHEM) spectrometer (Gloeckler et al., 1984) on the AMPTE Charge Composition Explorer (CCE) had this capability, measuring ion composition over the energy range 1-300 keV/e. The CCE was in an equatorial orbit with an 8.8 Re apogee, which leads to a significant amount of time spent in the near-earth plasma sheet. Thus it provides an ideal dataset to study the composition of the near-earth plasma sheet. The CCE launched in August 1984, and operated until 1989.

An estimate of the contribution of the two sources to the plasma sheet using the AMPTE measurements was reported in Gloeckler and Hamilton (1987). They assumed that the solar

wind composition did not change significantly in entering the magnetosphere and so the H^+/He^{++} and the $H^+/CNO^{>3+}$ ratios from the solar wind population remain within +/-50% of the average solar wind values, 25 and 1200, respectively. By measuring the densities for He^{++} and $CNO^{>3+}$, and assuming the solar wind ratios, they estimated the amount of the H^+ that comes from the solar wind. Knowing the fraction of H^+ that comes from the solar wind, they then assumed that the remainder of the H^+ comes from the ionosphere. They found that the ionospheric contribution to the plasma sheet was on average ~37% during quiet times and 65% during active times. This study was done using selected time periods early in the mission. No follow-up study was ever done to investigate the detailed time dependence of the source change, and in particular how the source changes during a storm. In this paper, we will use the composition measurements from AMPTE/CHEM to follow the source changes during a storm, to determine how the contributions from the solar wind and ionosphere change during the course of a storm.

2 Instrumentation

The CHEM instrument uses a combination of an electrostatic analyzer followed by post-acceleration, a time-of-flight measurement and an energy measurement to determine the mass and mass-per-charge of an ion. It covers the energy range 1-300 keV/e. The CCE was in an elliptical orbit with apogee at 8.8 Re. An example mass vs mass per charge matrix in the nightside outer magnetosphere ($L>7$) using this instrument can be seen in Christon et al., (1994), Plate 1. The instrument can distinguish individual charge states of the solar wind species, as well as separating N^+ from O^+ . The highest quality data is obtained using the detailed data from individual ions, rather than the count rates summed on board. However, the number of individual ion events included in the telemetry is limited, and so longer time averages are required to obtain statistically significant counts of the minor species. In this paper, we determine the detailed composition for hourly averages of data to track how the composition, and therefore the source, changes over the course of a storm. For the high charge state solar wind species, we combine the counts from carbon, nitrogen and oxygen with charge state $Q > 3$ in order to increase the statistics for the solar wind heavies. This data will be called $CNO^{>3+}$.

3 Data Analysis

Figure 1a shows the Sym-H index for the time period from 18-23 April 1985. A complex storm developed during this time. Beginning on the 19th, there was an increase in Sym-H, followed by a decrease signifying the storm main phase. Sym-H reached a minimum of -57 nT during this first main phase. At ~6:00 UT on the April 20th, there was a sharp increase, associated with a sudden commencement. In the last few hours of 20 April and into 21 April, a second main phase with a strong decrease down to -220 nT occurred.

The CCE orbit, shown on the right in Figure 1b, had an apogee at ~2:00 MLT during this storm. A spacecraft in this orbit spends a significant amount of time outside $L=6$, in the near-earth plasma sheet. Thus the transitions in the plasma sheet composition over the course of this storm can be explored.

Figure 1c shows a summary plot of one CCE orbit, perigee to perigee, from 22:30 on 18 April to 13:30 UT on 19 April. The time period, indicated with blue bar in figure 1a, includes the time Sym-H increases and the beginning of the first main phase. The top four panels give the differential number flux of H^+ , O^+ , He^+ and He^{++} during the orbit. The bottom panel shows the mass per charge of ions that are identified to have the mass of oxygen (left axis annotation) or

equivalently the charge state of oxygen (right axis annotation). The top line across this panel represents O^+ (mass per charge=16, $Q=1$), while the points towards the bottom represent the high charge state O^{+5} , O^{+6} , and O^{+7} (mass per charge between 2 and 2.7, $Q=5,6$ and 7). Between 1:00 and 11:00 UT on 18 April, the spacecraft is outside $L=6$, sampling the near-earth plasma sheet. There are three distinct composition changes during this time. From $\sim 1:00-4:00$, which corresponds to the SYM-H increase, there is a high intensity, low energy (<10 keV) H^+ population and a corresponding He^{++} population. The O^+ flux is very low during this time, and the oxygen charge states, shown on the bottom panel, are predominantly the solar wind high charge states. This population is clearly dominated by solar wind, a dense low-energy population with high charge state minor ions.

At $\sim 4:00$ UT, there is an increase in the more energetic ($\sim 10-50$ keV) H^+ and He^{++} , as well as an increase in O^+ in energies up to ~ 30 keV. The O^+ charge states now show both O^+ and some O^{++} , as well as the high charge state solar wind ions. Then, at $\sim 8:30$ UT, there is a second increase in H^+ and O^+ , now extending up to ~ 100 keV. This enhancement shows energy dispersed characteristics, particularly in the O^+ , with an enhancement observed first at higher energies, and then decreasing to lower energies. Now the charge state panel shows a more significant increase in the O^+ , and a reduced high charge state oxygen. Thus, during this orbit at the beginning of the storm, the composition changes from predominantly solar wind species, to a mixed population with a significant contribution from the ionosphere.

To examine this transition more quantitatively over the course of the storm, we have tracked how the densities of the different species change. Figure 2a shows the dipole L-value of the CCE orbit, from the 18 April through 22 April. The horizontal dashed line indicates $L=6$. Only data outside $L=6$ is shown in the following panels. Inside $L=6$, charge exchange can significantly alter the charge state distribution, which complicates the source population analysis, so we only use data outside $L=6$ to minimize that effect. The black lines in figure 2b, 2c, 2d, and 2f give the densities of H^+ , He^{++} , $CNO^{>3+}$, and O^+ . The density is calculated over the energy range 1-300 keV/e for 1-hour time intervals. Figure 2g shows the SYM-H index. Examination of the He^{++} and $CNO^{>3+}$ densities, the two solar wind origin species, shows very similar profiles, increasing and decreasing together a number of times during the storm as would be expected if they came from the same source. Figure 2e gives the ratio of the two densities, showing it is relatively constant. The O^+ profile in Figure 2f is completely different, starting low before the storm and then increasing as the SYM-H decreases, consistent with a population coming from a different source. The H^+ in Figure 2b (black line) has a profile somewhere between the solar wind ions and the O^+ , indicating that it is a mix, as expected. To determine the fraction of the H^+ that comes from the solar wind, we follow the method of Gloecker and Hamilton (1987), but use more recent solar wind data from Lepri et al., 2013, to determine the composition ratios. This April 1985 time period is in the solar minimum between solar cycles 21 and 22, so we use the solar minimum composition values. CME composition is more similar to slow wind composition, but with additional heavy ion enhancements. As a first check on using the Lepri et al. (2013) results we compare the $He^{++}/CNO^{>3+}$ ratio against that found by Lepri et al., (2013). Since both these species come from the solar wind, this ratio should agree with the solar wind value, independent of the ionospheric contribution. The red dashed line in Figure 2e shows the mean for this ratio for solar minimum slow solar wind from Lepri et al., (2013). The average during this storm is about 20.0, a little below the mean solar wind value of 25.8, closer to the 1-sigma level of 19.7. Because CMEs are expected to have enhanced heavy ions, we use the 1-sigma low values (ie. high heavy ion contribution) from Lepri for the H/CNO solar wind value,

with an error bar of +/- 50%. Lepri et al., 2013 does not include the Nitrogen abundance, so we assume that Nitrogen is 8.8% of Oxygen, based on Von Steiger et al. (2000). This gives an H/CNO value of 1089. We then use the measured average He⁺⁺/CNO of 20 to determine an H/He⁺⁺ value of 54. This is slightly higher than the Lepre et al. (2013) 1-sigma value of 32.47, but significantly below the mean value of 104.

Using these ratios, we calculate the estimated H⁺ from the solar wind. The red and green lines in Panel b show the estimated H⁺ from the solar wind based on the CNO^{>3+} (red) and the He⁺⁺ (green) measurements. The good agreement between the measured H⁺ profiles and the estimated H⁺ validate our approach. For the first few points at the beginning of 19 April, corresponding to the time when Sym-H increases prior to the first storm main phase, the estimated H⁺ is slightly higher than the measured H⁺, indicating that the solar wind heavy ion fraction during this time may be even higher than assumed. But for the rest of the storm, the H⁺ estimate is quite reasonable, agreeing with the measured value during some time periods, and falling well below for others. Before the storm, the H⁺ is consistent with a solar wind source. But as SYM-H starts to drop, the measured H⁺ density is higher than would be expected from just a solar wind source. The difference between the total H⁺ density and the solar wind contribution is the ionospheric contribution to the H⁺.

To determine the total amount of plasma coming from each source, we add the densities of the species from each source. This is shown in Figure 3. Figure 3a again shows the L-value of the spacecraft, and only data outside L=6 are included in the subsequent panels. Figure 3h again shows the SYM_H index to track the progress of the storm. Figure 3b shows the densities of the three most abundant ionospheric species, H⁺, O⁺ and N⁺. The ionospheric H⁺ component is determined by subtracting the solar wind H⁺ (using the CNO estimate) from the total. H⁺ remains the dominant ionospheric species in the plasma sheet throughout the storm, but as the storm develops the O⁺ and N⁺ densities increase. The total density from the ionosphere, adding all the ionospheric contributions, is shown in Figure 3c. Similarly Figure 3d shows the solar wind species. By definition, the H⁺ is always dominant here, as we are assuming that the solar wind contribution in the plasma sheet maintains its solar wind abundance, with an H⁺/He⁺⁺ ratio of 54. Therefore the total solar wind density, shown in Figure 3e is essentially the solar wind H⁺ density.

Figures 3f and 3g show the percent of the total from the ionosphere and the percent of the total from the solar wind as a function of time. Before the storm, the source is predominantly from the solar wind. As the Sym-H drops on 19 April, the ionospheric density increases and the solar wind density decreases, leading to a population dominated by the the ionospheric source. As the SYM-H levels out, and then increases during the sudden commencement on 20 April, the solar wind contribution increases significantly. The ionospheric contribution, particularly the O⁺, also increases during this time. In particular there is a strong increase in O⁺ just after 8:00 UT, likely associated with the sudden commencement, that leads to a mixed population, about 30% ionospheric and 70% solar wind. Then, as the Sym-H drops again, the solar wind contribution decreases while the ionospheric contribution increases, leading to a dominantly ionospheric population. Finally, during the recovery phase of the storm, during the second half of 21 April and into 22 April, the solar wind contribution increases again while the density from the ionospheric source, including the O⁺, decrease significantly, bringing the composition back to almost pure solar wind.

Thus, during this storm, the source of the near-earth plasma sheet population that supplies the ring current changes significantly. Prior to the storm, it is almost entirely H^+ from the solar wind. As SYM-H increases before the storm, the solar wind density peaks. As SYM-H drops, the solar wind component decreases and the ionospheric contribution increases. As the SYM-H levels out, the solar wind input increases again, so the population is mixed. It then drops as the SYM-H decreases again. During the recover phase, the solar wind source becomes dominant again.

In addition to the changing contributions of the two sources, the composition of the ionospheric source is also not constant during the storm. The heavy ion contribution of the ionospheric source increases during both main phases, and then drops in the recovery phase. In particular in the outbound pass starting at 16:00 on 21 April, the dominant source is still the ionosphere, but the O^+ contribution has decreased significantly. Thus, there are time periods when the O^+ density is low, but the source is ionospheric. Both changing source and changing source composition need to be considered in understanding the plasma sheet changes during a storm.

5 Conclusions

Our results have shown that the transport paths to the plasma sheet must change dramatically during a storm. At the very start of the storm, when the SYM-H increased, there was a dense solar wind population. This is consistent with the previous results of Thomsen et al. (2003) and Lavraud and Jordanova (2007) that suggested that the plasma sheet prior to the storm becomes cold, dense from plasma of solar wind origin. However, as the main phase begins, ionospheric plasma is transported to the near-earth plasma sheet, and becomes the dominant population. At the end of the main phase, when the SYM_H levels out or increases, the source population changes back to solar wind. This transition occurs twice during this double-dip storm.

While there is no simultaneous IMF data available during this time period, it is reasonable to suggest that these dramatic changes in transport are related to the changes in the IMF direction. It is well known that the main phase occurs when the IMF turns southward. This southward orientation changes the convection, bringing the ionospheric ions into the plasma sheet. Similarly, it has been shown that during northward IMF, solar wind plasma enters the magnetosphere, both through dayside reconnection in the cusp region and at the flanks, populating the plasma sheet. A geomagnetic storm is characterized by the transitions between these two modes of ion access to the plasma sheet. These data show that the transitions occur quickly enough to change the near-earth plasma sheet composition early in the main phase. This transition can explain how the ionospheric species, particularly O^+ , become significant contributors to the storm-time ring current.

Acknowledgments and Data

Work at UNH was supported by NASA grant 80NSSC19K0073. The AMPTE/CHEM data is available from the JHU/APL AMPTE/CCE Science Data Center, at <http://sd-www.jhuapl.edu/AMPTE/chem/data/>.

References

- Christon, S. P., Hamilton, D. C., Gloeckler, G., & Eastmann, T. E. (1994). High charge state carbon and oxygen ions in Earth's equatorial quasi-trapping region. *Journal of Geophysical Research*, *99*, 13465. <http://doi.org/10.1029/93JA03328>
- Engwall, E., Eriksson, A. I., André, M., Dandouras, I., Paschmann, G., Quinn, J., & Torkar, K. (2006). Low-energy (order 10 eV) ion flow in the magnetotail lobes inferred from spacecraft wake observations. *Geophysical Research Letters*, *33*(6), 6110. <http://doi.org/10.1029/2005GL025179>
- Galvin, A. B. (1997). Minor ion composition in CME-related solar wind. *Coronal Mass Ejections*. (1997), *99*, 253–260. <http://doi.org/10.1029/GM099p0253>
- Gloeckler, G., Ipavich, F. M., Hamilton, D. C., Lundgren, R. A., Studemann, W., Wilken, B., et al. (1985). The charge-energy-mass spectrometer for 0.3-300 keV/e ions on the AMPTE CCE. *IEEE Transactions on Geoscience and Remote Sensing (ISSN 0196-2892)*, *23*, 234–240. <http://doi.org/10.1109/TGRS.1985.289519>
- Gloeckler, G., & Hamilton, D. C. (1987). AMPTE ion composition results. *Scostep*, *18*, 73–84. <http://doi.org/10.1088/0031-8949/1987/T18/009>
- Greenspan, M. E., & Hamilton, D. C. (2002). Relative contributions of H⁺ and O⁺ to the ring current energy near magnetic storm maximum. *Journal of Geophysical Research (Space Physics)*, *107*(A), 1043. <http://doi.org/10.1029/2001JA000155>
- Hamilton, D. C., Gloeckler, G., Ipavich, F. M., Wilken, B., Studemann, W., Wilken, B., & Kremser, G. (1988). Ring current development during the great geomagnetic storm of February 1986. *Journal of Geophysical Research*, *93*, 14343–14355. <http://doi.org/10.1029/JA093iA12p14343>
- Kasper, J. C., Stevens, M. L., Lazarus, A. J., Steinberg, J. T., & Ogilvie, K. W. (2007). Solar Wind Helium Abundance as a Function of Speed and Heliographic Latitude: Variation through a Solar Cycle. *The Astrophysical Journal*, *660*(1), 901–910. <http://doi.org/10.1086/510842>
- Kasper, J. C., Stevens, M. L., Korreck, K. E., Maruca, B. A., Kiefer, K. K., Schwadron, N. A., & Lepri, S. T. (2012). Evolution of the Relationships between Helium Abundance, Minor Ion Charge State, and Solar Wind Speed over the Solar Cycle. *The Astrophysical Journal*, *745*(2), 162. <http://doi.org/10.1088/0004-637X/745/2/162>
- Kistler, L. M., Mouikis, C. G., Klecker, B., & Dandouras, I. (2010). Cusp as a source for oxygen in the plasma sheet during geomagnetic storms. *Journal of Geophysical Research*, *115*(A), 03209. <http://doi.org/10.1029/2009JA014838>
- Kistler, L. M., Mouikis, C. G., Spence, H. E., Menz, A. M., Skoug, R. M., Funsten, H. O., et al. (2016). The source of O⁺ in the storm time ring current. *Journal of Geophysical Research (Space Physics)*, *121*(6), 5333–5349. <http://doi.org/10.1002/2015JA022204>
- Kistler, L. M., Mouikis, C. G., Asamura, K., Yokota, S., Kasahara, S., Miyoshi, Y., et al. (2019). Cusp and Nightside Auroral Sources of O⁺ in the Plasma Sheet. *Journal of Geophysical Research (Space Physics)*, *124*(1), 10–. <http://doi.org/10.1029/2019JA027061>

- Lavraud, B., & Jordanova, V. K. (2007). Modeling the effects of cold-dense and hot-tenuous plasma sheet on proton ring current energy and peak location. *Geophysical Research Letters*, *34*, L02102–. <http://doi.org/10.1029/2006GL027566>.
- Lepri, S. T., Landi, E., & Zurbuchen, T. H. (2013). Solar Wind Heavy Ions over Solar Cycle 23: ACE/SWICS Measurements. *The Astrophysical Journal*, *768*(1), 94. <http://doi.org/10.1088/0004-637X/768/1/94>.
- Li, K., Haaland, S., Eriksson, A., André, M., Engwall, E., Wei, Y., et al. (2012). On the ionospheric source region of cold ion outflow. *Geophysical Research Letters*, *39*(1), 18102. <http://doi.org/10.1029/2012GL053297>.
- Li, K., Haaland, S., Eriksson, A., André, M., Engwall, E., Wei, Y., et al. (2013). Transport of cold ions from the polar ionosphere to the plasma sheet. *Journal of Geophysical Research (Space Physics)*, *118*(9), 5467–5477. <http://doi.org/10.1002/jgra.50518>.
- Liao, J., Kistler, L. M., Mouikis, C. G., Klecker, B., Dandouras, I., & Zhang, J.-C. (2010). Statistical study of O⁺ transport from the cusp to the lobes with Cluster CODIF data. *Journal of Geophysical Research*, *115*. <http://doi.org/10.1029/2010JA015613>.
- Mouikis, C. G., Kistler, L. M., Liu, Y. H., Klecker, B., Korth, A., & Dandouras, I. (2010). H⁺ and O⁺ content of the plasma sheet at 15–19 Re as a function of geomagnetic and solar activity. *Journal of Geophysical Research*, *115*, A00J16. <http://doi.org/10.1029/2010JA015978>.
- Mouikis, C. G., Bingham, S. T., Kistler, L. M., Farrugia, C. J., Spence, H. E., Reeves, G. D., et al. (2019). The Storm-Time Ring Current Response to ICMEs and CIRs Using Van Allen Probe Observations. *Journal of Geophysical Research (Space Physics)*, *124*(1), 9017–9039. <http://doi.org/10.1029/2019JA026695>.
- Øieroset, M., Phan, T. D., Fujimoto, M., Chan, L., Lin, R. P., & Skoug, R. (2003). Spatial and temporal variations of the cold dense plasma sheet: Evidence for a low-latitude boundary layer source? *Earth's Low-Latitude Boundary Layer. (2003)*, *133*, 253–264. <http://doi.org/10.1029/133GM25>.
- Sorathia, K. A., Merkin, V. G., Ukhorskiy, A. Y., Allen, R. C., Nykyri, K., & Wing, S. (2019). Solar Wind Ion Entry Into the Magnetosphere During Northward IMF. *Journal of Geophysical Research (Space Physics)*, *124*(7), 5461–5481. <http://doi.org/10.1029/2019JA026728>.
- Thomsen, M. F., Borovsky, J. E., Skoug, R. M., & Smith, C. W. (2003). Delivery of cold, dense plasma sheet material into the near-Earth region. *Journal of Geophysical Research (Space Physics)*, *108*(A), 1151. <http://doi.org/10.1029/2002JA009544>.
- von Steiger, R., Schwadron, N. A., Fisk, L. A., Geiss, J., Gloeckler, G., Hefti, S., et al. (2000). Composition of quasi-stationary solar wind flows from Ulysses/Solar Wind Ion Composition Spectrometer. *Journal of Geophysical Research*, *105*(A), 27217–27238. <http://doi.org/10.1029/1999JA000358>
- Wilson, G. R. (2004). Nightside auroral zone and polar cap ion outflow as a function of substorm size and phase. *Journal of Geophysical Research*, *109*(A2), A02206. <http://doi.org/10.1029/2003JA009835>

Wing, S., Johnson, J. R., Chaston, C. C., Echim, M., Escoubet, C. P., Lavraud, B., et al. (2014). Review of Solar Wind Entry into and Transport Within the Plasma Sheet. *Space Science Reviews*, 184(1), 33–86. <http://doi.org/10.1007/s11214-014-0108-9>.

Yau, A. W., & André, M. (1997). Sources of Ion Outflow in the High Latitude Ionosphere. *Space Science Reviews*, 80(1), 1–25. <http://doi.org/10.1023/A:1004947203046>.

Yau, A. W., Abe, T., & Peterson, W. K. (2007). The polar wind: Recent observations. *Journal of Atmospheric and Solar-Terrestrial Physics*, 69(1), 1936–1983. <http://doi.org/10.1016/j.jastp.2007.08.010>

Young, D. T., Balsiger, H., & Geiss, J. (1982). Correlations of magnetospheric ion composition with geomagnetic and solar activity. *Journal of Geophysical Research*, 87, 9077–9096. <http://doi.org/10.1029/JA087iA11p09077>.

Zhao, K., Kistler, L. M., Lund, E. J., Nowrouzi, N., Kitamura, N., & Strangeway, R. J. (2020). Factors controlling O⁺ and H⁺ outflow in the cusp during a geomagnetic storm: FAST/TEAMS observations. *Geophysical Research Letters*, 46, e2020GL086975. <https://doi.org/10.1029/2020GL086975>.

Zurbuchen, T. H., & Richardson, I. G. (2006). In-Situ Solar Wind and Magnetic Field Signatures of Interplanetary Coronal Mass Ejections. *Space Science Reviews*, 123(1), 31–43. <http://doi.org/10.1007/s11214-006-9010-4>.

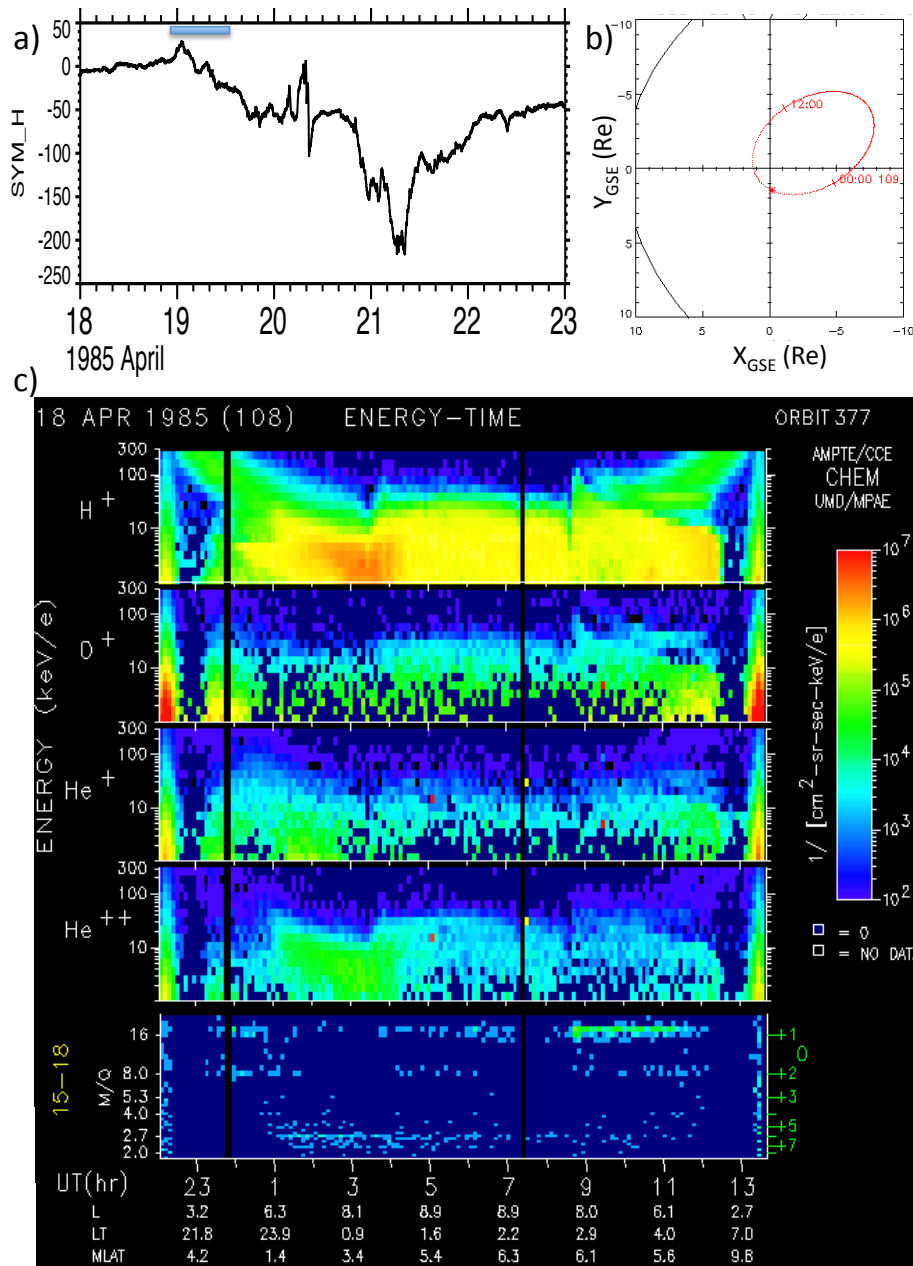


Figure 1. a) Sym-H index from 18 April 1985 through 22 April 1985. Blue bar indicates the time periods of the orbit shown in c). b) Orbit of the AMPTE/CCE spacecraft during this storm c) One orbit of AMPTE/CCE data showing H^+ , O^+ , He^+ and He^{++} differential flux as a function of energy per charge, and the charge state of the oxygen ions measured.

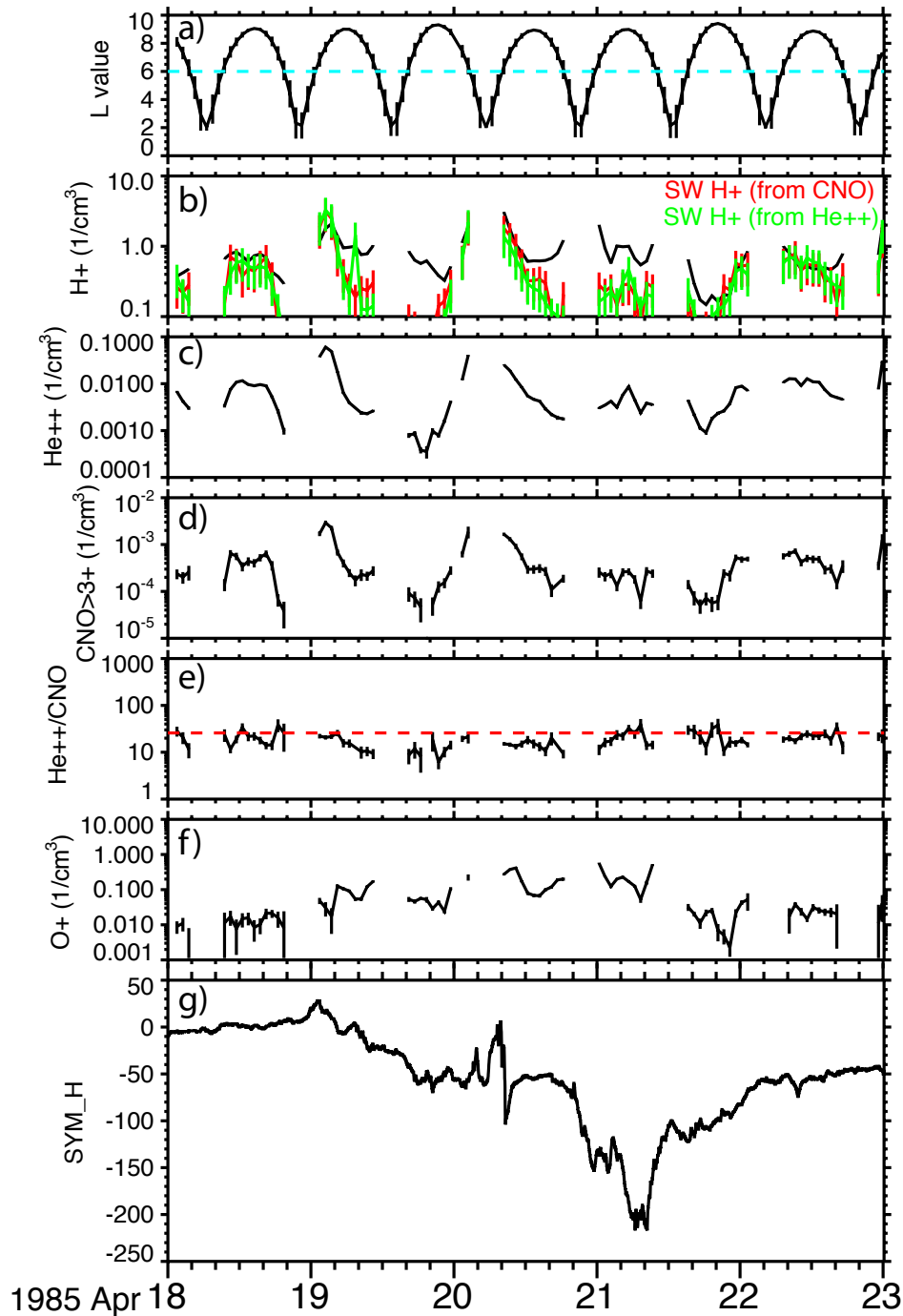


Figure 2. a) Dipole L-value at the CCE location. The dashed line marks $L=6$. For panels b) through f), only data outside $L=6$ is shown. b) H^+ density. Black is the measured density. Red and green are the estimated solar wind H^+ density, using the $CNO>3^+$ measurements and the He^{++} measurements. c) He^{++} density d) $CNO>3^+$ density e) $He^{++}/CNO>3^+$ ratio f) O^+ density g) SYM-H index.

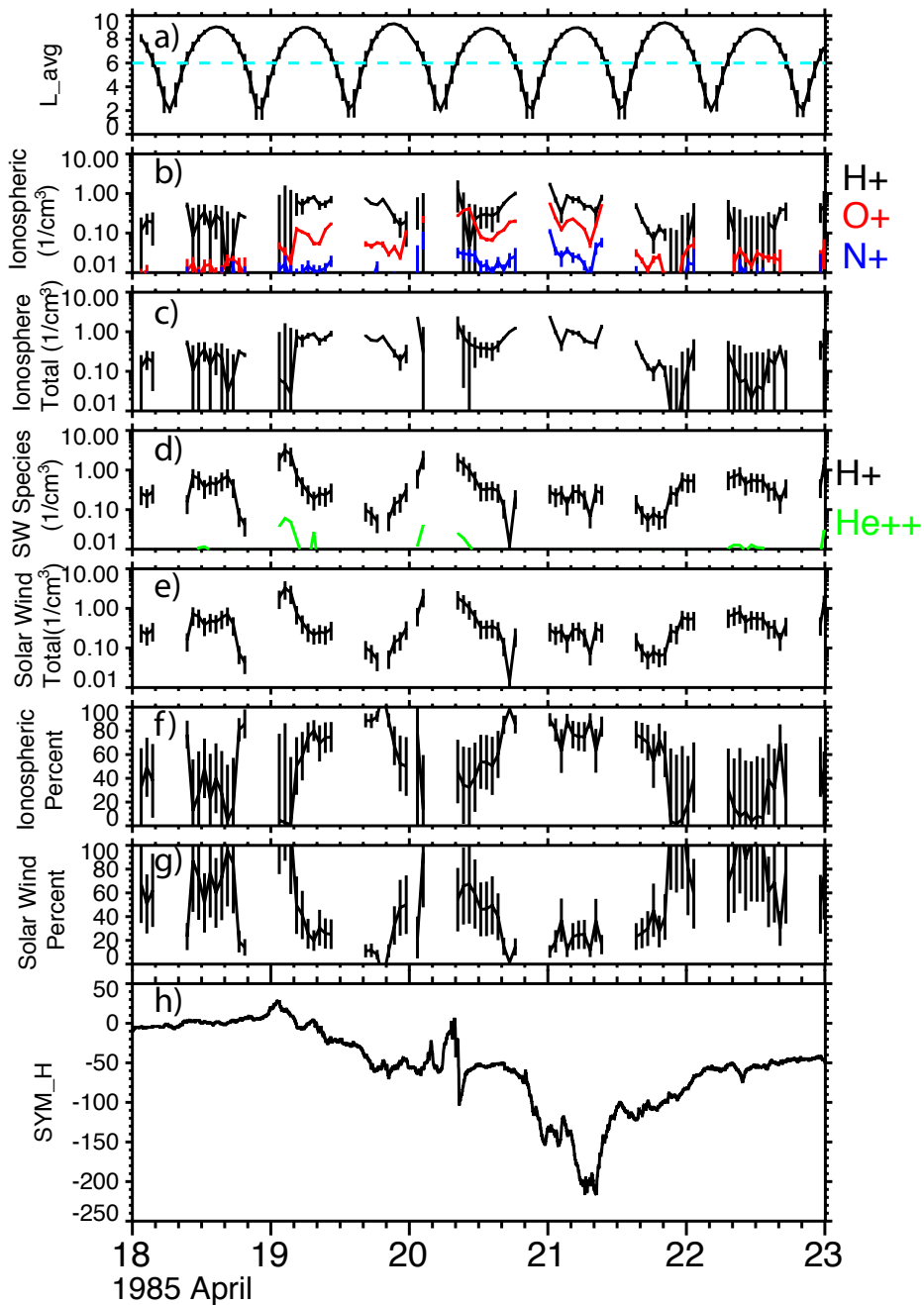


Figure 3. a) Dipole L-value at the CCE location. The dashed line marks $L=6$. For panels b) through g), only data outside $L=6$ is shown. b) Density of H^+ , O^+ and N^+ from the ionospheric source. c) Total density from the ionospheric source. d) Density of H^+ and He^{++} from the solar wind source. e) Total density from the solar wind source. f) Percent of the total density from the ionospheric source. g) Percent of the total density from the solar wind source. h) SYM-H index.